0.01%) (Fig. 6F). This similarity of the mean magnitude difference for normal and low BP further demonstrates the preserved orientation selectivity at low BP. Taken together with the similarity of preferred orientation spiking activity for both BP conditions (Fig. 4C), these data suggest that the dHb change in *blood* measured by 620-nm OIS reflects increases of oxygen consumption in *neurons*. Thus, spatial specificity inherent in dHb signals can be examined during the low BP condition because only the CBF and CBV responses induced by neural activity are minimized.

Time-dependent spatial specificity of deoxyhemoglobin and CBV signals

To examine the spatial specificity of OIS, we separately calculated time courses of OIS within active and inactive domains from the single-condition raw activity maps (Figs. 7A and B). Whether the stimulus-induced reflection changes at 620 nm were positive or negative, similar magnitudes of reflection changes were observed at all time points in both the active and inactive domains at normal BP (Fig. 7A, red and blue lines in left panel). Interestingly, signal magnitudes of the two domains at 620 nm were similar even at the low BP conditions (Fig. 7A, right panel). Since stimulation-induced changes in blood velocity and volume were reduced significantly during the low BP conditions, the 620-nm OIS observed in both domains is not likely to be due to widespread dHb changes caused by CBF and CBV responses or light scattering (Ls) induced by velocity changes (Tomita et al., 1983), but rather caused by widespread dHb content changes per se. Similar magnitudes of reflection changes in active and inactive domains were also observed at 570 nm (Fig. 7B), where the signal source is CBV weighted. It should be noted that our selection of active and inactive column ROIs is based on conventional optical imaging approaches. If a higher threshold (such as a z score of 2) is used for the decision of ROIs, the signal difference between the active and inactive ROIs (green lines in Fig. 7) is larger; in present studies, the signal difference between active and in-active domains is the smallest. However, its time-dependent characteristics remain the same.

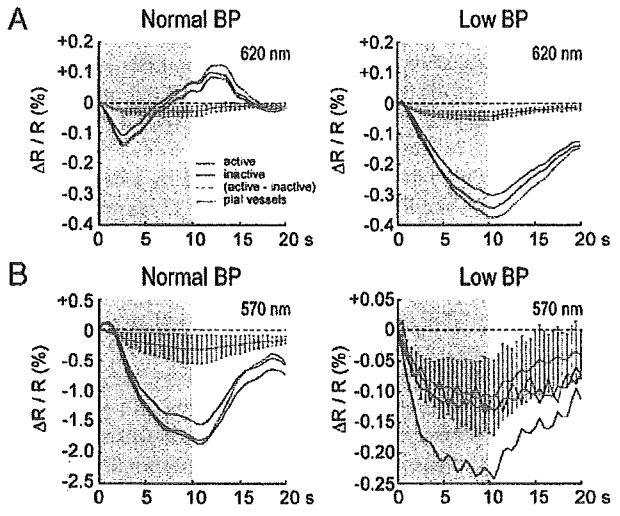

Fig. 7. Time courses of dHb and CBV signals from active and inactive domains. (A) Average time courses of the 620-nm OIS (n = 5 cats) for normal (left panel) and low (right panel) BP conditions. The red and blue lines depict reflection changes for active and inactive domains, respectively. The green line represents changes in 'active domain' (red line) minus changes in 'inactive domain' (blue line). The black dotted line indicates the reflection changes in pial vessels. Error bars of green lines are ±1 SD. (B) Average time courses of the 570-nm OIS (n = 5 cats) for normal BP (left panel) and low BP (right panel) conditions. Color representations are the same as for panel A.

Before reporting quantitative results of the spatial specificity, the "sensitivity" and "specificity" of the OIS signal have to be defined (see also discussion in Duong et al., 2000a). Fig. 8A shows two hypothetical OIS profiles (S1 and S2, blue and red solid lines respectively) from single-condition raw activity maps, in which two neighboring iso-orientation domains (gray areas in *A*) are activated simultaneously. OIS activation area is much larger than column size determined by neural spike activity (black bars in *A*); OIS is induced even in orthogonal orientation columns (between two gray areas in *A*). Thus, OIS consists of orientation-non-specific and -specific signals. Typically, when two orthogonal stimuli are employed, orientation-non-specific signals have been determined by cocktail blank analysis. Analogous to this, the orientation-non-specific component is obtained from an average of signals between the iso-orientation and orthogonal domains (DC_1 and DC_2, blue and red dotted lines respectively). "Sensitivity" to detect a column is determined by the magnitude of the orientation-specific modulations (ΔS_1 and ΔS_2). To compare the sensitivity of S1 and S2, the orientation-non-specific modulations (DC_1 and DC_2) are subtracted from the raw OIS profiles (S1 and S2). As in Fig. 8B, the S1 sensitivity is larger than the S2 ($\Delta S_1 > \Delta S_2$). However, larger sensitivity does not necessary mean better spatial specificity; the non-specific modulation should also be considered. The "specificity" of the signal is related to the signal point spread, which is generally determined by the full-width at half-maximum (FWHM) of the signal. To compare the FWHM of the S1 and S2, each with different magnitude, the peak of S1 and S2 is normalized to 1.0. As in Fig. 8C, the profile of the S1 is broader than that of the S2. Thus, the FWHM of the S2 (a red horizontal bar) is smaller than that of the S1 (a blue horizontal bar); the specificity of the S2 is better than that of the S1. Instead of FWHM, the normalized sensitivity ($\Delta S'_1$ and $\Delta S'_2$) can be used as an index of FWHM because it is correlated with FWHM (i.e., $\Delta S'_1 < \Delta S'_2$; larger value, better specificity). However, normalization by the signal peak is not practical for the OIS raw activity maps because signal magnitudes are different among iso-orientation domains (e.g., see Fig. 8G). Thus, we used the orientation-non-specific signal for normalization instead (Fig. 8D); the orientation-specific modulation (Fig. 8B) is divided by the non-specific modulation (DC_1 and DC_2 in Fig. 8A). We will refer to this ratio ($\Delta S/DC$) as spatial specificity index (larger ratio, better specificity). As consistent to the Fig. 8C ($\Delta S'_1 < \Delta S'_2$), the spatial specificity index of the S2 is larger than that of the S1 ($\Delta S_1/DC_1 < \Delta S_2/DC_2$), suggesting better spatial specificity of the S2 compared to the S1 (Fig. 8D).

Actual OIS profiles (a 620-nm OIS with low BP) corresponding to Figs. 8A–D are shown in Figs. 8E–H. OIS profiles from single-condition raw activity maps at three different time periods (average for 1–2, 4–6, and 8–10 s) were plotted in Fig. 8E (thick solid lines, raw signals; thin solid lines, low-pass filtered (cutoff frequency, 1.5 Hz) signals). Dotted lines are the orientation-non-specific modulations, which were obtained from "single-condition raw activity maps" minus "single-condition iso-orientation maps". The arrow indicates the location of a column (see Fig. 9A). Both orientation-

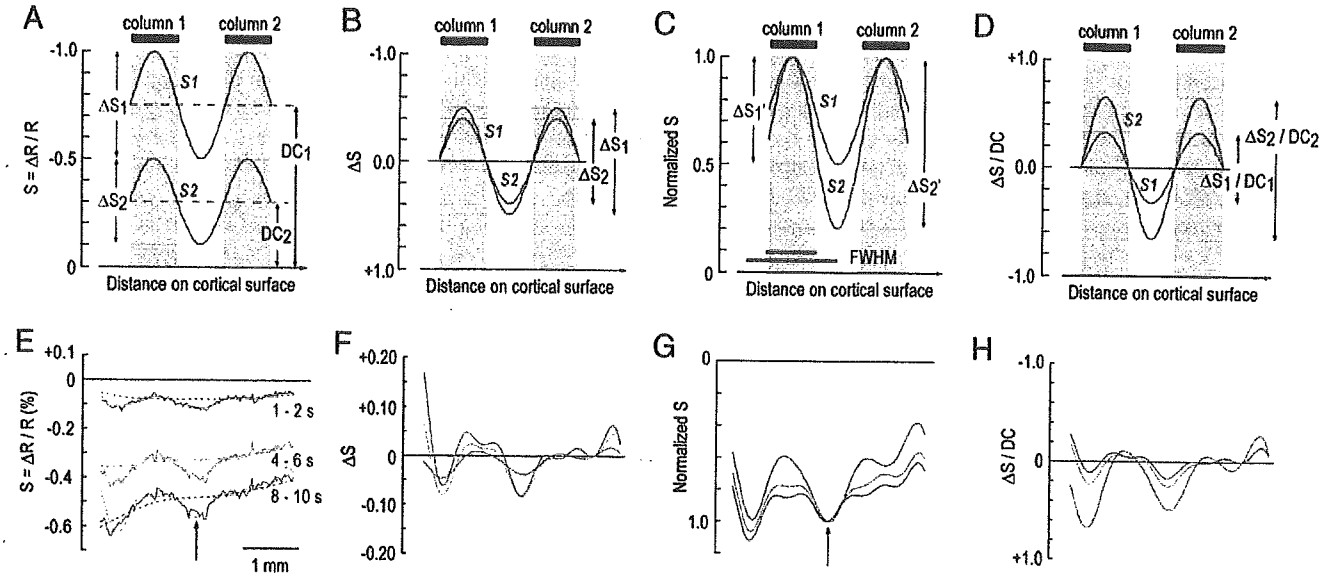

Fig. 8. Definition of sensitivity and specificity. (A–D) OIS profiles from hypothetical data. (E–H) OIS Profiles corresponding to panels (A–D) from actual data (620-nm OIS with low BP) obtained from the region between two dashed lines in Fig. 9A. (A) Two OIS profiles (solid blue (S1) and red (S2) lines) obtained from hypothetical single-condition raw activity maps. Dotted blue and red lines are orientation-non-specific modulations of each OIS. Gray areas are the column size determined by neural spike activity (black bars). (B) Orientation-specific modulation parts (ΔS_1 and ΔS_2) are extracted from the raw OIS signals (S1 and S2) by subtracting the orientation-non-specific modulations (DC_1 and DC_2). (C) Normalized raw OIS profiles. The raw OIS profiles shown in panel A (S1 and S2) are normalized by their peak values in the iso-orientation domains (gray areas). Horizontal blue and red bars are the FWHM of S1 and S2, respectively. After normalization, $\Delta S'_1$ and $\Delta S'_2$ can be used as an index for the FWHM of S1 and S2. (D) Normalized orientation-specific modulations. The orientation-specific modulations shown in panel B (ΔS_1 and ΔS_2) are normalized by the non-specific modulations (DC_1 and DC_2). This ratio (ΔS/DC) is referred to as spatial specificity index. (E) Profiles of single-condition raw activity maps from 620-nm OIS with low BP at three different time periods (1–2 s, 4–6 s, and 8–10 s, red, green, and blue respectively). Thin solid lines superimposed on raw signals (thick solid lines) are OIS profiles after removing high frequency noise by a filter (cutoff 1.5 Hz), which are used for analyses in panels F–H. Dotted lines indicate orientation-non-specific modulations. The arrow indicates the location of an iso-orientation domain. The scale bar and the line colors are applicable to panels E–H. (F) Profiles of orientation-specific modulation parts. (G) Profiles of OIS normalized by a peak indicated by the arrow. (H) Profiles of the orientation-specific modulation parts (F) normalized by the orientation-non-specific components (dotted lines in panel E).

non-specific (dotted lines in Fig. 8E) and -specific (Fig. 8F) modulations developed with time. To compare FWHM of the raw OIS signals, the peak of all three profiles indicated by the arrow was normalized to 1.0 (Fig. 8G). In the normalized profiles, the spread of OIS became larger with time. In accordance with this, the spatial specificity index (ΔS/DC) became smaller over time (Fig. 8H).

The maps corresponding to Figs. 8F (sensitivity) and H (spatial specificity index) are shown in upper and lower panels in Fig. 9A, respectively. The sensitivity map is equivalent to the single-condition iso-orientation map (i.e., the orientation-non-specific signal is removed). The specificity index map is obtained from dividing the sensitivity map by an orientation-non-specific map (i.e., the "single-condition raw activity map" minus the "single-condition iso-orientation map"). Higher contrasts of iso-orientation domains in sensitivity and specificity index maps indicate higher sensitivity and specificity, respectively. As in upper panels of Fig. 9A, the iso-orientation domains in the sensitivity maps were clearer in later time points, suggesting the sensitivity became larger with time. On the other hand, the iso-orientation domains in the spatial specificity index maps (Fig. 9A lower panels) were clearer at an early time point (1–2 s) compared to later time points (4–6 and 8–10 s), suggesting the spatial specificity became poor with time. Pial draining vessels' responses were also apparent at later time points. For comparison, sensitivity and specificity index maps for a 570-nm OIS with low BP are shown in upper and lower panels of Fig. 9B. As similar to the 620-nm OIS with low BP, the signal sensitivity changed with time: it improved. In contrast, the spatial specificity index of the 570-nm OIS with low BP did not seem to change much over time. Pial draining vessels' responses were also not apparent even at later time points.

We finally quantify the average spatial specificity index for 620-nm OIS ($n = 5$ cats) and for 570-nm OIS ($n = 4$ of 5 cats, one cat was excluded from the analysis because of low SNR) at each time point and plot them as a function of time from the stimulus onset (Fig. 10). Since multiple components probably contribute to the OIS at normal BP, each with a different sensitivity and specificity, we only quantified the sensitivity and specificity of OIS at low BP. To obtain the index, the difference in OIS magnitudes between the active and inactive domains (corresponding to the sensitivity (ΔS); green lines in Figs. 7A and B) was divided by the average in OIS magnitude between the active and inactive domains (corresponding to the orientation-non-specific component (DC)). Thus, when the signal is only observed in the active domains, the index will be 2.0. On the other hand, when the magnitude of the signal in the active domains is the same as that in the inactive domains, the index will be 0. Results with one-way repeated measures ANOVA indicated a statistically significant difference among times during a 10-s visual stimulation ($F_{18,72} = 8.122$, $P = 3.73 \times 10^{-11}$) for the 620-nm OIS. During the low BP condition, the average spatial specificity index of the 620-nm OIS for all five cats (red line in Fig. 10A) was initially as high as 0.86 ± 0.60 (at 1.0 s after the stimulus onset) and quickly declined with time (statistically significant differences between the indices at

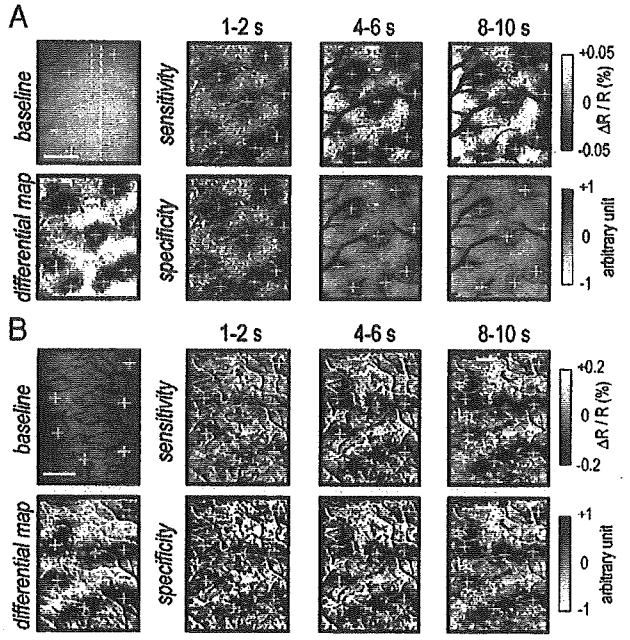

Fig. 9. Sensitivity and spatial specificity index maps at progressive time points. (A) Spatiotemporal patterns of the low BP 620-nm OIS from an illustrative study. A cortical surface image at 620 nm (baseline image) shows pial vessels for sensitivity maps (upper) and spatial specificity index maps (lower) for a 10-s visual stimulation with a grating orientation of 45° at 1–2, 4–6, and 8–10 s from stimulus onset. The scale bar is 1 mm. The data are from the same study as Figs. 8E–H. Yellow crosses on the panels indicate location of black patches selective to the 45° orientation, which were determined from the differential iso-orientation map at 620 nm (differential map). Specificity indices were 0.28, 0.11, and 0.07, while sensitivities were 0.02, 0.04, and 0.04% at progressive time points. (B) Spatiotemporal patterns of the low BP 570-nm OIS from an illustrative study. Specificity indices were 0.66, 0.63, and 0.53, while sensitivities were 0.06, 0.12, and 0.12% at progressive time points. Stimulus orientation used was 0°. Wavelength used was 570 nm except the differential map (620 nm). Other conventions are the same as panel A.

two successive times were $P = 0.001–0.049$). This spatial specificity dependence on time cannot be explained by the scattering of light, which is inherent in optical measurement (Orbach and Cohen, 1983), because scattering of light originating from the active domains to inactive domains should be closely correlated, resulting in time-independent spatial specificity. By contrast, the index of the 570-nm OIS with low BP (blue line in Fig. 10A) did not show such a time variance during a 10-s visual stimulation (results with one-way repeated measures ANOVA indicated no statistically significant difference among times ($F_{18,72} = 0.482$, $P = 0.955$). On the other hand, the sensitivity of the 620-nm OIS during low BP (green line in Fig. 10B) became better at later time points, whereas the specificity became poor (orange line in Fig. 10B). To visualize iso-orientation domains, there is a trade off between the specificity and the sensitivity; specificity is high while sensitivity is poor or vice versa.

Discussion

We have demonstrated during low BP conditions (i) the stimulus-induced CBV response is reduced without changing neural activity, and (ii) time-dependent spatial specificity of dHb responses to active orientation-selective columns. During visual stimulation under sNP-induced low BP conditions with vessel dilation, the dHb content change (620-nm OIS) resulting from the increase in oxygen consumption can be separated from the effect of CBF and CBV changes (570-nm OIS). Consequently, a prolonged dip was observed in the 620-nm OIS during a 10-s stimulation period. A similar observation was found in fMRI studies in this laboratory (Nagaoka et al., 2002, in press), where positive BOLD signals during normal BP conditions changed into negative BOLD signals at low BP. Thus, current dHb-weighted 620-nm and CBV-weighted 570-nm OIS studies are directly applicable to the investigation of spatial specificity of fMRI at a columnar level.

Utilization of sNP-induced low blood pressure

The sNP is widely clinically used to reduce blood pressure. Even at less than 50 mm Hg MABP, the following physiological parameters were well maintained; cortical surface oxygen tension (Maekawa et al., 1979 (cat)), $CMRO_2$ (Michenfelder and Milde, 1988 (dog); Pinaud et al., 1989 (human); Schumann-Bard et al., 2005; Schumann et al., 1998 (baboon)), pH and normal ionic concentration gradients across cell membranes (Morris et al., 1983 (cat)), evoked field potential (Kottenberg-Assenmacher et al., 2003 (human)), and the power of EEG (Ishikawa and McDowall, 1980 (cat)). Here, we have also demonstrated good maintenance of orientation-specific spiking activity (see Fig. 4) and dHb signal (see Fig. 6) during sNP-induced low BP. The reduction of evoked-CBV (the present study) and CBF (Artru and Colley, 1984; Gregory et al., 1981) during sNP-induced low BP seems to be larger than those caused by nitric oxide synthetase (NOS) inhibitors (e.g., Offenhauser et al., 2005; for review, see Iadecola and Niwa, 2002). Thus, instead of use of NOS inhibitors, sNP-induced low BP can be used for a considerable reduction of evoked CBV and CBF responses without concomitant decrease of neural activity.

One concern for sNP administration is cyanide toxicity. However, McDowall et al. (1974) reported no toxicity (i.e., "the animals showing a normal response") for baboon in the use of 1.25 $mg \cdot kg^{-1} \cdot h^{-1}$ (Table 2 in McDowall et al., 1974). Similarly, cyanide toxicity does not seem to be represented in cat at <1 mg/kg sNP administration (Ishikawa and McDowall, 1980; Maekawa et al., 1979; Morris et al., 1983). Because our total dosage of sNP was

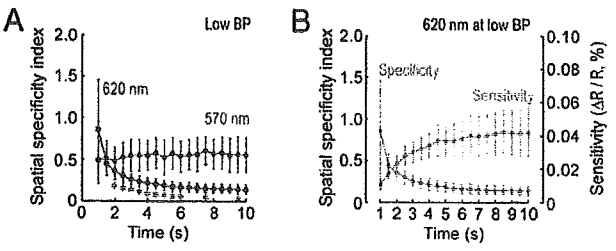

Fig. 10. Time-dependent spatial specificity and sensitivity of dHb and CBV signals. (A) Average time courses of spatial specificity index for the 570-nm (blue) and 620-nm OIS (red) in low BP conditions. The indices at 0 and 0.5 s were not calculated due to poor SNR. Error bars are ±1 SD ($n = 5$ for the 620-nm OIS; $n = 4$ for the 570-nm OIS). Asterisks (*) indicate a statistically significant difference ($P < 0.05$) between two successive time points. (B) Spatial specificity index (orange line) vs. sensitivity (green line) for 620-nm OIS during low BP. The data in panel A (red line) and Fig. 7A (green line) are used for demonstration. Error bars are ±1 SD.

less than 1 mg/kg, cyanide toxicity in our preparation may not be significant. Another concern is that nitric oxide (NO) is generated from sNP administration. Because in addition to its vasodilation effect, NO also inhibits cytochrome oxidase (Brown and Cooper, 1994) and thus during sNP administration $CMRO_2$ is possibly reduced despite unchanged spiking activity. Maekawa et al. (1979) reported a modest decrease of $CMRO_2$ even in an adequate oxygen supply during sNP-induced low BP. However, even if $CMRO_2$ decreases during sNP administration, as long as dHb is produced by oxygen consumption, time-dependent spatial specificity of dHb signal should be preserved.

What makes spatial specificity of deoxyhemoglobin signals poor?

The aim of this study was to determine spatial specificity of the dHb signal inherently induced by oxygen consumption. Even though the effect of CBF and CBV changes on the dHb signal was considerably reduced, the spatial specificity of 620-nm OIS to the iso-orientation domains was good only during the initial few seconds (see Figs. 9 and 10). This finding suggests that the poor spatial specificity of the dHb signal at later time points during the low BP condition is not due to widespread dHb changes caused by CBF or CBV modulations but is rather caused directly by widespread changes in the dHb signal itself. Two possible explanations could account for the time-dependent decrease in spatial specificity of the dHb signal at low BP.

First, if the wide extent of the OIS is tied to the wide distribution of sub-threshold synaptic activity (Grinvald et al., 1994; Sharon and Grinvald, 2002) or lateral spread of spiking activity along dendrites and axonal processes, the spatial specificity of the dHb signal will be poor. Since OIS signals are elicited by changes in spiking activity or synaptic potentials of neurons (Das and Gilbert, 1995; Gurden et al., 2003; Kinoshita et al., 2003; Toth et al., 1996) or both, it is plausible that the spread of neural activity over time could cause a time-dependent spread of intrinsic signals (for example, see Liu et al., 2003). Further studies are necessary to determine the neural origin of OIS.

Second, we propose that draining of dHb from active sites can easily explain the time-dependent spread of the 620-nm OIS at low BP. Even though neural origin of the OIS remains controversial, changes in oxygen consumption and glucose metabolism seem to occur within the active iso-orientation domain and not the inactive domain (Lowel et al., 1987; Thompson et al., 2003). Then dHb produced by oxygen consumption increases within active domains should drain into downstream vessels, including intracortical and pial veins, due to the existence of blood flow even though a stimulation-evoked CBF change is not induced (referred to draining effect).

For image detection of the draining effect, the distance between intracortical veins must be less than the size of the functional column. Density of emerging veins ($\sim$2.5/mm^2; inter-vessel distance, $\sim$0.6 mm, estimated by Fig. 63 in Duvernoy et al. (1981) and Park et al., 2005) is approximately two times higher than that of iso-orientation domains ($\sim$1.2/mm^2, inter-columnar distance: $\sim$1.0 mm) for a single orientation (Bonhoeffer and Grinvald, 1993; Rao et al., 1997). If dHb induced by neural activity initially increases within active iso-orientation domains and then drains into the intracortical emerging veins, dHb-based signals may not originate from the 'true' active domains. Furthermore, pial venous networks are highly dense, suggesting that dHb changes will eventually spread over the cortical surface, and reducing the signal specificity further. Consequently, the 620-nm OIS at low BP would lose its specificity with time.

Dynamic 620-nm OIS changes in tissue and in pial vessels were almost identical (see Fig. 5D). This suggests that the draining of dHb from active domains into the pial vessels is faster than our sampling rate (0.5 s). Taking into account that the arteriovenous transit time of red blood cells is 0.1–0.35 s (Hudetz, 1997; Rovainen et al., 1993 in rodents), dHb changes in tissue regions will be quickly integrated into an emerging vein and spread into pial veins within 1 s (see also Narayan et al., 1994; Takashima et al., 2001). Thus, only the early time point (up to $\sim$2 s) of the 620-nm OIS dip is specific to active regions.

Spatial specificity of CBV-weighted signals

At normal BP conditions, local CBV changes elicited by neural activity have to occur in concert with dilation in upstream parent arteries (Erinjeri and Woolsey, 2002; Iadecola et al., 1997). To reduce the less-specific vascular contributions from upstream arteries, post-processing analyses were applied to CBV-weighted OIS studies of rodent barrel cortex (Hess et al., 2000; Sheth et al., 2004), and cat and primate visual cortex (Vanzetta et al., 2004). Then CBV changes in parenchymal microvessels (diameter $< \sim$10 μm) were found to be specific to sub-millimeter functional domains (Frostig et al., 1990; Fukuda et al., 2005; Hess et al., 2000; Narayan et al., 1995; Sheth et al., 2004; Vanzetta et al., 2004). After this removal of signal contribution from pial arteries, CBV-weighted signals originate from penetrating arterioles, branching small arterioles and possibly capillaries. If penetrating arterioles are individually controlled, their density defines the limit for CBV-weighted spatial resolution. The density of penetrating arterioles (15.8/mm^2, inter-arteriole distance: $\sim$0.25 mm) in the cat cerebral cortex (McHedlishvili and Kuridze, 1984) is much higher than that of iso-orientation domains (1.2/mm^2, inter-domain distance: $\sim$1.0 mm). Thus, detection of penetrating arterioles would provide sufficient resolution for mapping iso-orientation domains in cats. If CBV regulation occurs within smaller-size vessels including capillaries, then an even higher spatial resolution can be achieved.

Reducing arterial BP decreased the less-specific vascular contributions from upstream arteries. The 570-nm OIS almost disappeared at low BP except for a component highly localized to iso-orientation domains (see Fig. 9B). We suggest that this remaining component is also due to CBV changes in parenchymal microvessels rather than changes in Ls due to cellular swelling (Holthoff and Witte, 1996; MacVicar and Hochman, 1991) because the activity-dependent Ls component is unlikely to significantly contribute to the OIS in vivo (Nomura et al., 2000). Since, unlike pial vessels, parenchymal vessels may not be fully dilated at low BP, they can still respond to stimulus (for CO_2 stimulation, see Gregory et al., 1981), suggesting CBV regulation within parenchymal microvessels independently of parent artery.

Implication for columnar resolution functional MRI

Our results suggest that the draining effect of pial and intracortical veins in dHb-based imaging techniques is intrinsically unavoidable (Figs. 5 and 7; see also Hayashi et al., 2005) and reduces its spatial specificity of dHb signal (Figs. 9 and 10); it appears immediately after the stimulus onset ($\sim$2 s) and becomes dominant with time. Similarly, Duong et al. (2000a) reported that

only the first ~2 s of the entire early negative BOLD response at normal BP showed high spatial specificity to cats' iso-orientation columns; Kim et al. (2000a) used the first 2-s BOLD dip for mapping iso-orientation domains in cats. Positive BOLD data acquired before the draining effect become significant (e.g., less than 2–4 s from stimulus onset) was shown to improve spatial specificity (Goodyear and Menon, 2001; Menon and Goodyear, 1999). Thus, regardless of the BOLD signal polarity (negative or positive), only data obtained within a few seconds after the onset of stimulation (i.e., before the draining effect dominates) can be used for high-resolution studies if the non-specific signal from pial and intra-cortical draining vessels is not removed. Once the non-specific signal is removed, a longer stimulation duration can be applied to increase the sensitivity of signals (i.e., difference between active and inactive domains) (Fig. 8D, see also Cheng et al., 2001).

To reduce the non-specific signals and consequently improve the spatial specificity in primary visual cortex where the cortical modules from orthogonal stimuli have a complementary pattern (e.g., ocular dominance and iso-orientation domains), the non-specific components in optical imaging studies have been removed by (i) the subtraction of imaging signals in response to orthogonal stimuli (Blasdel, 1992; Blasdel and Salama, 1986; Grinvald et al., 1986; for review, see Bonhoeffer and Grinvald, 1996), and (ii) Fourier analysis of data acquired during repeated orthogonal stimuli (Kalatsky and Stryker, 2003). Similar approaches were used to map human ocular dominance columns with positive BOLD (Cheng et al., 2001; Menon et al., 1997). However, the differential methods cannot be applied to most brain areas because orthogonal stimulation condition is unknown. Thus, the single-condition map has to be used.

Positive BOLD signal at normal BP is derived from a mismatch between $CMRO_2$ and CBF changes. Thus, besides the draining effect, the specificity and sensitivity of BOLD signal are determined by a combination of $CMRO_2$ and CBF responses. Since an increase in $CMRO_2$ causes a decrease in BOLD signal, while an increase in CBF causes an increase in BOLD signal, the specificity and sensitivity of BOLD signal are possibly poorer than that of either $CMRO_2$ or CBF signals (see also Duong et al., 2000a). Thus, alternative non-BOLD fMRI methods, which have high sensitivity and are free from complication by the draining effect, should be considered for single-condition stimulation. Based on our 570-nm OIS results, we suggest that CBV-weighted fMRI (Belliveau et al., 1991; Kennan et al., 1998; Mandeville et al., 1998; van Bruggen et al., 1998) and possibly CBF-weighted fMRI (Edelman et al., 1994; Kim, 1995; Kwong et al., 1992) will have an improved spatial specificity of hemodynamic signals. Unlike the 570-nm OIS, both CBV- and CBF-weighted fMRI can minimize the contribution of large pial vessels even at normal BP (Duong et al., 2000b; Mandeville and Marota, 1999; Silva et al., 2000) and have been successfully applied to laminar (Harel et al., 2002b; Duong et al., 2000b; Lu et al., 2004; Zhao et al., 2004b) and columnar resolution fMRI studies (Duong et al., 2001; Zhao et al., 2005) in the cat visual cortex.

Acknowledgments

We thank Kristy Hendrich, Michelle Tasker, and Toshihiro Hayashi for their helpful comments on the manuscript. This study was supported by NIH EB003324, EB003375, EB002013, NS44589 and McKnight Foundation.

References

Artru, A.A., Colley, P.S., 1984. Cerebral blood flow responses to hypocapnia during hypotension. Stroke 15 (5), 878–883.

Belliveau, J.W., Kennedy Jr., D.N., McKinstry, R.C., Buchbinder, B.R., Weisskoff, R.M., Cohen, M.S., Vevea, J.M., Brady, T.J., Rosen, B.R., 1991. Functional mapping of the human visual cortex by magnetic resonance imaging. Science 254 (5032), 716–719.

Bishop, P.O., Kozak, W., Vakkur, G.J., 1962. Some quantitative aspects of the cat's eye: axis and plane of reference, visual field co-ordinates and optics. J. Physiol. 163, 466–502.

Blasdel, G.G., 1992. Differential imaging of ocular dominance and orientation selectivity in monkey striate cortex. J. Neurosci. 12 (8), 3115–3138.

Blasdel, G.G., Salama, G., 1986. Voltage-sensitive dyes reveal a modular organization in monkey striate cortex. Nature 321 (6070), 579–585.

Bonhoeffer, T., Grinvald, A., 1993. The layout of iso-orientation domains in area 18 of cat visual cortex: optical imaging reveals a pinwheel-like organization. J. Neurosci. 13 (10), 4157–4180.

Bonhoeffer, T., Grinvald, A., 1996. Optical imaging based on intrinsic signals: the methodology. In: Toga, A.W., Mazziotta, J.C. (Eds.), Brain Mapping: The Methods. Academic, San Diego, pp. 55–97.

Bonhoeffer, T., Kim, D.S., Malonek, D., Shoham, D., Grinvald, A., 1995. Optical imaging of the layout of functional domains in area 17 and across the area 17/18 border in cat visual cortex. Eur. J. Neurosci. 7 (9), 1973–1988.

Brown, G.C., Cooper, C.E., 1994. Nanomolar concentrations of nitric oxide reversibly inhibit synaptosomal respiration by competing with oxygen at cytochrome oxidase. FEBS Lett. 356 (2–3), 295–298.

Buxton, R.B., 2001. The elusive initial dip. NeuroImage 13 (6 Pt. 1), 953–958.

Cheng, K., Waggoner, R.A., Tanaka, K., 2001. Human ocular dominance columns as revealed by high-field functional magnetic resonance imaging. Neuron 32 (2), 359–374.

Chillon, J.-M., Baumbach, G.L., 2002. Autoregulation: arterial and intracranial pressure. In: Edvinsson, L., Krause, D.N. (Eds.), Cerebral Blood Flow and Metabolism, 2nd ed. Lippincott Williams and Wilkins, Philadelphia, pp. 395–412.

Das, A., Gilbert, C.D., 1995. Long-range horizontal connections and their role in cortical reorganization revealed by optical recording of cat primary visual cortex. Nature 375 (6534), 780–784.

Duong, T.Q., Kim, D.S., Ugurbil, K., Kim, S.G., 2000a. Spatiotemporal dynamics of the BOLD fMRI signals: toward mapping submillimeter cortical columns using the early negative response. Magn. Reson. Med. 44 (2), 231–242.

Duong, T.Q., Silva, A.C., Lee, S.P., Kim, S.G., 2000b. Functional MRI of calcium-dependent synaptic activity: cross correlation with CBF and BOLD measurements. Magn. Reson. Med. 43 (3), 383–392.

Duong, T.Q., Kim, D.S., Ugurbil, K., Kim, S.G., 2001. Localized cerebral blood flow response at submillimeter columnar resolution. Proc. Natl. Acad. Sci. U. S. A. 98 (19), 10904–10909.

Duvernoy, H.M., Delon, S., Vannson, J.L., 1981. Cortical blood vessels of the human brain. Brain Res. Bull. 7 (5), 519–579.

Edelman, R.R., Gaa, J., Wedeen, V.J., Loh, E., Hare, J.M., Prasad, P., Li, W., 1994. In vivo measurement of water diffusion in the human heart. Magn. Reson. Med. 32 (3), 423–428.

Endrich, B., Franke, N., Peter, K., Messmer, K., 1987. Induced hypotension: action of sodium nitroprusside and nitroglycerin on the microcirculation. A micropuncture investigation. Anesthesiology 66 (5), 605–613.

Erinjeri, J.P., Woolsey, T.A., 2002. Spatial integration of vascular changes with neural activity in mouse cortex. J. Cereb. Blood Flow Metab. 22 (3), 353–360.

Ferrari, M., Wilson, D.A., Hanley, D.F., Traystman, R.J., 1992. Effects of graded hypotension on cerebral blood flow, blood volume, and mean transit time in dogs. Am. J. Physiol. 262 (6 Pt. 2), H1908–H1914.

Fox, P.T., Raichle, M.E., 1986. Focal physiological uncoupling of cerebral blood flow and oxidative metabolism during somatosensory stimulation in human subjects. Proc. Natl. Acad. Sci. U. S. A. 83 (4), 1140–1144.

Frostig, R.D., Lieke, E.E., Ts'o, D.Y., Grinvald, A., 1990. Cortical functional architecture and local coupling between neuronal activity and the microcirculation revealed by in vivo high-resolution optical imaging of intrinsic signals. Proc. Natl. Acad. Sci. U. S. A. 87 (16), 6082–6086.

Fukuda, M., Rajagopalan, U.M., Homma, R., Matsumoto, M., Nishizaki, M., Tanifuji, M., 2005. Localization of activity-dependent changes in blood volume to submillimeter-scale functional domains in cat visual cortex. Cereb. Cortex 15 (6), 823–833.

Goodyear, B.G., Menon, R.S., 2001. Brief visual stimulation allows mapping of ocular dominance in visual cortex using fMRI. Hum. Brain Mapp. 14 (4), 210–217.

Gregory, P., Ishikawa, T., McDowall, D.G., 1981. CO2 responses of the cerebral circulation during drug-induced hypotension in the cat. J. Cereb. Blood Flow Metab. 1 (2), 195–201.

Grinvald, A., Lieke, E., Frostig, R.D., Gilbert, C.D., Wiesel, T.N., 1986. Functional architecture of cortex revealed by optical imaging of intrinsic signals. Nature 324 (6095), 361–364.

Grinvald, A., Lieke, E.E., Frostig, R.D., Hildesheim, R., 1994. Cortical point-spread function and long-range lateral interactions revealed by real-time optical imaging of macaque monkey primary visual cortex. J. Neurosci. 14 (5 Pt. 1), 2545–2568.

Grinvald, A., Slovin, H., Vanzetta, I., 2000. Non-invasive visualization of cortical columns by fMRI. Nat. Neurosci. 3 (2), 105–107.

Gurden, H., Uchida, N., Mainen, Z., 2003. Presynaptic origin of odor-evoked intrinsic signal in olfactory glomeruli. Abstr. - Soc. Neurosci. 33, 489.5.

Harel, N., Lee, S.P., Nagaoka, T., Kim, D.S., Kim, S.G., 2002a. Origin of negative blood oxygenation level-dependent fMRI signals. J. Cereb. Blood Flow Metab. 22 (8), 908–917.

Harel, N., Zhao, F., Wang, P., Kim, S.-G., 2002b. Layer Specificity of BOLD and CBV fMRI Signals At Ultra-High Resolution. 8th International Conference on Functional Mapping of the Human Brain.

Hayashi, T., Park, S.-H., Kim, S.-G., 2005. Relationship between intracortical vascular architecture and functional activation foci in high-resolution BOLD fMRI. 11th International Conference on Functional Mapping of the Human Brain.

Hennig, J., Ernst, T., Speck, O., Deuschl, G., Feifel, E., 1994. Detection of brain activation using oxygenation sensitive functional spectroscopy. Magn. Reson. Med. 31 (1), 85–90.

Hess, A., Stiller, D., Kaulisch, T., Heil, P., Scheich, H., 2000. New insights into the hemodynamic blood oxygenation level-dependent response through combination of functional magnetic resonance imaging and optical recording in gerbil barrel cortex. J. Neurosci. 20 (9), 3328–3338.

Holthoff, K., Witte, O.W., 1996. Intrinsic optical signals in rat neocortical slices measured with near-infrared dark-field microscopy reveal changes in extracellular space. J. Neurosci. 16 (8), 2740–2749.

Hu, X., Le, T.H., Ugurbil, K., 1997. Evaluation of the early response in fMRI in individual subjects using short stimulus duration. Magn. Reson. Med. 37 (6), 877–884.

Hudetz, A.G., 1997. Blood flow in the cerebral capillary network: a review emphasizing observations with intravital microscopy. Microcirculation 4 (2), 233–252.

Iadecola, C., Niwa, K., 2002. Nitric oxide. In: Edvinsson, L., Krause, D.N. (Eds.), Cerebral Blood Flow and Metabolism, 2nd ed. Lippincott Williams and Wilkins, Philadelphia, pp. 295–310.

Iadecola, C., Yang, G., Ebner, T.J., Chen, G., 1997. Local and propagated vascular responses evoked by focal synaptic activity in cerebellar cortex. J. Neurophysiol. 78 (2), 651–659.

Ishikawa, T., McDowall, D.G., 1980. Electrical activity of the cerebral cortex during induced hypotension with sodium nitroprusside and trimetaphan in the cat. Br. J. Anaesth. 53 (6), 605–611.

Issa, N.P., Trepel, C., Stryker, M.P., 2000. Spatial frequency maps in cat visual cortex. J. Neurosci. 20 (22), 8504–8514.

Jezzard, P., Rauschecker, J.P., Malonek, D., 1997. An in vivo model for functional MRI in cat visual cortex. Magn. Reson. Med. 38 (5), 699–705.

Kalatsky, V.A., Stryker, M.P., 2003. New paradigm for optical imaging: temporally encoded maps of intrinsic signal. Neuron 38 (4), 529–545.

Kennan, R.P., Scanley, B.E., Innis, R.B., Gore, J.C., 1998. Physiological basis for BOLD MR signal changes due to neuronal stimulation: separation of blood volume and magnetic susceptibility effects. Magn. Reson. Med. 40 (6), 840–846.

Kim, S.G., 1995. Quantification of relative cerebral blood flow change by flow-sensitive alternating inversion recovery (FAIR) technique: application to functional mapping. Magn. Reson. Med. 34 (3), 293–301.

Kim, D.S., Duong, T.Q., Kim, S.G., 2000a. High-resolution mapping of iso-orientation columns by fMRI. Nat. Neurosci. 3 (2), 164–169.

Kim, D.S., Duong, T.Q., Kim, S.G., 2000b. Reply to "Can current fMRI techniques reveal the micro-architecture of cortex?" Nat. Neurosci. 3 (5), 414.

Kinoshita, M., Gilbert, C.D., Das, A., 2003. Optical imaging of contextual interactions in V1 of the behaving monkey. Abstr. - Soc. Neurosci. 33, 484.5.

Kontos, H.A., Wei, E.P., Navari, R.M., Levasseur, J.E., Rosenblum, W.I., Patterson Jr., J.L., 1978. Responses of cerebral arteries and arterioles to acute hypotension and hypertension. Am. J. Physiol. 234 (4), H371–H383.

Kottenberg-Assenmacher, E., Armbruster, W., Bornfeld, N., Peters, J., 2003. Hypothermia does not alter somatosensory evoked potential amplitude and global cerebral oxygen extraction during marked sodium nitroprusside-induced arterial hypotension. Anesthesiology 98 (5), 1112–1118.

Kwong, K.K., Belliveau, J.W., Chesler, D.A., Goldberg, I.E., Weisskoff, R.M., Poncelet, B.P., Kennedy, D.N., Hoppel, B.E., Cohen, M.S., Turner, R., et al., 1992. Dynamic magnetic resonance imaging of human brain activity during primary sensory stimulation. Proc. Natl. Acad. Sci. U. S. A. 89 (12), 5675–5679.

Lindauer, U., Royl, G., Leithner, C., Kuhl, M., Gold, L., Gethmann, J., Kohl-Bareis, M., Villringer, A., Dirnagl, U., 2001. No evidence for early decrease in blood oxygenation in rat whisker cortex in response to functional activation. NeuroImage 13 (6), 988–1001.

Liu, G.B., Zhang, Y., Pettigrew, J.D., Xu, W.F., Li, C.Y., 2003. Spreading and synchronization of intrinsic signals in visual cortex of macaque monkey evoked by a localized visual stimulus. Brain Res. 985 (1), 13–20.

Logothetis, N., 2000. Can current fMRI techniques reveal the micro-architecture of cortex? Nat. Neurosci. 3 (5), 413–414.

Lowel, S., Freeman, B., Singer, W., 1987. Topographic organization of the orientation column system in large flat-mounts of the cat visual cortex: a 2-deoxyglucose study. J. Comp. Neurol. 255 (3), 401–415.

Lu, H., Patel, S., Luo, F., Li, S.J., Hillard, C.J., Ward, B.D., Hyde, J.S., 2004. Spatial correlations of laminar BOLD and CBV responses to rat whisker stimulation with neuronal activity localized by Fos expression. Magn. Reson. Med. 52 (5), 1060–1068.

MacVicar, B.A., Hochman, D., 1991. Imaging of synaptically evoked intrinsic optical signals in hippocampal slices. J. Neurosci. 11 (5), 1458–1469.

Maekawa, T., McDowall, D.G., Okuda, Y., 1979. Brain-surface oxygen tension and cerebral cortical blood flow during hemorrhagic and drug-induced hypotension in the cat. Anesthesiology 51 (4), 313–320.

Malonek, D., Grinvald, A., 1996. Interactions between electrical activity and cortical microcirculation revealed by imaging spectroscopy: implications for functional brain mapping. Science 272 (5261), 551–554.

Mandeville, J.B., Marota, J.J., 1999. Vascular filters of functional MRI: spatial localization using BOLD and CBV contrast. Magn. Reson. Med. 42 (3), 591–598.

Mandeville, J.B., Marota, J.J., Kosofsky, B.E., Keltner, J.R., Weissleder, R., Rosen, B.R., Weisskoff, R.M., 1998. Dynamic functional imaging of relative cerebral blood volume during rat forepaw stimulation. Magn. Reson. Med. 39 (4), 615–624.

Mayhew, J.E., Askew, S., Zheng, Y., Porrill, J., Westby, G.W., Redgrave, P., Rector, D.M., Harper, R.M., 1996. Cerebral vasomotion: a 0.1-Hz oscillation in reflected light imaging of neural activity. NeuroImage 4 (3 Pt. 1), 183–193.

McDowall, D.G., Keaney, N.P., Turner, J.M., Lane, J.R., Okuda, Y., 1974. The toxicity of sodium nitroprusside. Br. J. Anaesth. 46 (5), 327–332.

McHedlishvili, G., Kuridze, N., 1984. The modular organization of the pial arterial system in phylogeny. J. Cereb. Blood Flow Metab. 4 (3), 391–396.

Menon, R.S., Goodyear, B.G., 1999. Submillimeter functional localization in human striate cortex using BOLD contrast at 4 Tesla: implications for the vascular point-spread function. Magn. Reson. Med. 41 (2), 230–235.

Menon, R.S., Ogawa, S., Hu, X., Strupp, J.P., Anderson, P., Ugurbil, K., 1995. BOLD based functional MRI at 4 Tesla includes a capillary bed contribution: echo-planar imaging correlates with previous optical imaging using intrinsic signals. Magn. Reson. Med. 33 (3), 453–459.

Menon, R.S., Ogawa, S., Strupp, J.P., Ugurbil, K., 1997. Ocular dominance in human V1 demonstrated by functional magnetic resonance imaging. J. Neurophysiol. 77 (5), 2780–2787.

Michenfelder, J.D., Milde, J.H., 1988. The interaction of sodium nitroprusside, hypotension, and isoflurane in determining cerebral vasculature effects. Anesthesiology 69 (6), 870–875.

Morris, P.J., Heuser, D., McDowall, D.G., Hashiba, M., Myers, D., 1983. Cerebral cortical extracellular fluid H+ and K+ activities during hypotension in cats. Anesthesiology 59 (1), 10–18.

Nagaoka, T., Harel, N., Zhao, F., Wang, P., Kim, S.G., 2002. Critical threshold of arterial blood pressure for BOLD responses to visual stimulation in anesthetized cats. Proc. Int. Soc. Mag. Reson., 10.

Nagaoka, T., Zhao, F., Wang, P., Harel, N., Kennan, R.P., Ogawa, S., Kim, S.G., in press. Increases in oxygen consumption without cerebral blood volume change during visual stimulation under hypotension condition, J. Cereb. Blood Flow Metab.

Narayan, S.M., Santori, E.M., Blood, A.J., Burton, J.S., Toga, A.W., 1994. Imaging optical reflectance in rodent barrel and forelimb sensory cortex. NeuroImage 1 (3), 181–190.

Narayan, S.M., Esfahani, P., Blood, A.J., Sikkens, L., Toga, A.W., 1995. Functional increases in cerebral blood volume over somatosensory cortex. J. Cereb. Blood Flow Metab. 15 (5), 754–765.

Nomura, Y., Fujii, F., Sato, C., Nemoto, M., Tamura, M., 2000. Exchange transfusion with fluorocarbon for studying synaptically evoked optical signal in rat cortex. Brain Res. Brain Res. Protoc. 5 (1), 10–15.

Offenhauser, N., Thomsen, K., Caesar, K., Lauritzen, M., 2005. Activity-induced tissue oxygenation changes in rat cerebellar cortex: interplay of postsynaptic activation and blood flow. J. Physiol. 565 (Pt. 1), 279–294.

Ogawa, S., Lee, T.M., Kay, A.R., Tank, D.W., 1990. Brain magnetic resonance imaging with contrast dependent on blood oxygenation. Proc. Natl. Acad. Sci. U. S. A. 87 (24), 9868–9872.

Orbach, H.S., Cohen, L.B., 1983. Optical monitoring of activity from many areas of the in vitro and in vivo salamander olfactory bulb: a new method for studying functional organization in the vertebrate central nervous system. J. Neurosci. 3 (11), 2251–2262.

Park, S.-H., Hayashi, T., Kim, S.-G., 2005. Determination of intracortical venous vessel density using venography at 9.4 T. Proc. Int. Soc. Magn. Reson., 13.

Pinaud, M., Souron, R., Lelausque, J.N., Gazeau, M.F., Lajat, Y., Dixneuf, B., 1989. Cerebral blood flow and cerebral oxygen consumption during nitroprusside-induced hypotension to less than 50 mmHg. Anesthesiology 70 (2), 255–260.

Rao, S.C., Toth, L.J., Sur, M., 1997. Optically imaged maps of orientation preference in primary visual cortex of cats and ferrets. J. Comp. Neurol. 387 (3), 358–370.

Ratzlaff, E.H., Grinvald, A., 1991. A tandem-lens epifluorescence macroscope: hundred-fold brightness advantage for wide-field imaging. J. Neurosci. Methods 36 (2–3), 127–137.

Rovainen, C.M., Woolsey, T.A., Blocher, N.C., Wang, D.B., Robinson, O.F., 1993. Blood flow in single surface arterioles and venules on the mouse somatosensory cortex measured with videomicroscopy, fluorescent dextrans, nonoccluding fluorescent beads, and computer-assisted image analysis. J. Cereb. Blood Flow Metab. 13 (3), 359–371.

Sato, M., Pawlik, G., Umbach, C., Heiss, W.D., 1984. Comparative studies of regional CNS blood flow and evoked potentials in the cat. Effects of hypotensive ischemia on somatosensory evoked potentials in cerebral cortex and spinal cord. Stroke 15 (1), 97–101.

Schumann, P., Touzani, O., Young, A.R., Morello, R., Baron, J.C., MacKenzie, E.T., 1998. Evaluation of the ratio of cerebral blood flow to cerebral blood volume as an index of local cerebral perfusion pressure. Brain 121 (Pt. 7), 1369–1379.

Schumann-Bard, P., Touzani, O., Young, A.R., Toutain, J., Baron, J.C., Mackenzie, E.T., Schmidt, E.A., 2005. Cerebrovascular effects of sodium nitroprusside in the anaesthetized baboon: a positron emission tomographic study. J. Cereb. Blood Flow Metab. 25 (4), 535–544.

Sharon, D., Grinvald, A., 2002. Dynamics and constancy in cortical spatiotemporal patterns of orientation processing. Science 295 (5554), 512–515.

Sheth, S.A., Nemoto, M., Guiou, M., Walker, M., Pouratian, N., Hageman, N., Toga, A.W., Sheth, S., 2004. Columnar specificity of microvascular oxygenation and volume responses: implications for functional brain mapping. J. Neurosci. 24 (3), 634–641.

Shmuel, A., Grinvald, A., 1996. Functional organization for direction of motion and its relationship to orientation maps in cat area 18. J. Neurosci. 16 (21), 6945–6964.

Silva, A.C., Lee, S.P., Iadecola, C., Kim, S.G., 2000. Early temporal characteristics of cerebral blood flow and deoxyhemoglobin changes during somatosensory stimulation. J. Cereb. Blood Flow Metab. 20 (1), 201–206.

Takashima, I., Kajiwara, R., Iijima, T., 2001. Voltage-sensitive dye versus intrinsic signal optical imaging: comparison of optically determined functional maps from rat barrel cortex. NeuroReport 12 (13), 2889–2894.

Thompson, J.K., Peterson, M.R., Freeman, R.D., 2003. Single-neuron activity and tissue oxygenation in the cerebral cortex. Science 299 (5609), 1070–1072.

Tomita, M., Gotoh, F., Yamamoto, M., Tanahashi, N., Kobari, M., 1983. Effects of hemolysis, hematocrit, RBC swelling, and flow rate on light scattering by blood in a 0.26 cm ID transparent tube. Biorheology 20 (5), 485–494.

Toth, L.J., Rao, S.C., Kim, D.S., Somers, D., Sur, M., 1996. Subthreshold facilitation and suppression in primary visual cortex revealed by intrinsic signal imaging. Proc. Natl. Acad. Sci. U. S. A. 93 (18), 9869–9874.

Tusa, R.J., Rosenquist, A.C., Palmer, L.A., 1979. Retinotopic organization of areas 18 and 19 in the cat. J. Comp. Neurol. 185 (4), 657–678.

van Bruggen, N., Busch, E., Palmer, J.T., Williams, S.P., de Crespigny, A.J., 1998. High-resolution functional magnetic resonance imaging of the rat brain: mapping changes in cerebral blood volume using iron oxide contrast media. J. Cereb. Blood Flow Metab. 18 (11), 1178–1183.

Vanzetta, I., Grinvald, A., 1999. Increased cortical oxidative metabolism due to sensory stimulation: implications for functional brain imaging. Science 286 (5444), 1555–1558.

Vanzetta, I., Slovin, H., Omer, D.B., Grinvald, A., 2004. Columnar resolution of blood volume and oximetry functional maps in the behaving monkey; implications for fMRI. Neuron 42 (5), 843–854.

Woolsey, T.A., Rovainen, C.M., Cox, S.B., Henegar, M.H., Liang, G.E., Liu, D., Moskalenko, Y.E., Sui, J., Wei, L., 1996. Neuronal units linked to microvascular modules in cerebral cortex: response elements for imaging the brain. Cereb. Cortex 6 (5), 647–660.

Zhao, F., Wang, P., Kim, S.G., 2004a. Cortical depth-dependent gradient-echo and spin-echo BOLD fMRI at 9.4 T. Magn. Reson. Med. 51 (3), 518–524.

Zhao, F., Wang, P., Ugurbil, K., Kim, S.G., 2004b. Cortical layer-dependent basal CBV and stimulation-induced CBV responses. Proc. Int. Soc. Mag. Reson., 12.

Zhao, F., Wang, P., Hendrich, K., Kim, S.-G., 2005. Spatial specificity of cerebral blood volume-weighted fMRI responses at columnar resolution. NeuroImage 27 (2), 416–424.

Representation of object images by combinations of visual features in the macaque inferior temporal cortex

Manabu Tanifuji*, Kazushige Tsunoda*[1] and Yukako Yamane*[2]

**Laboratory for Integrative Neural Systems, Brain Science Institute, The Institute of Physical and Chemical Research (RIKEN), Hirosawa 2-1, Wako-shi, Saitama 351-0198, Japan*

Abstract. The ventral visual pathway is essential for object recognition where features necessary for recognition are extracted from object images. This pathway is not directly related to action; nevertheless extraction of features from object images through this pathway is closely related to actions since we determine our behaviour based on sensory information, such as object images in the scene. To link perception and action, we have investigated neural representation of object images in area TE. Area TE, the anterior part of the inferior temporal (IT) cortex, is the final purely visual area in the ventral visual pathway. Since individual neurons in this area respond to features less complex than object images, an object image is supposed to be represented by multiple features. Here, to investigate sets of features necessary for representation of object images, we conducted a combination study of an optical imaging technique and single cellular recordings from anesthetized macaque monkeys.

2005 Percept, decision, action: bridging the gaps. Wiley, Chichester (Novartis Foundation Symposium 270) p 217–231

Visual features represented by neurons in area TE

It is known that neurons in this area respond to object images but also to visual features that are geometrically less complex than the object images (Desimone et al 1984, Tanaka et al 1991, Kobatake & Tanaka 1994). In particular, Tanaka and colleagues examined responses of neurons in area TE with systematically simplified visual stimuli and found that visual stimuli sufficient to activate many neurons were moderately complex visual features that are less complex than object images ('critical feature') (Kobatake & Tanaka 1994) (e.g. see Fig. 1). Many of these features are

[1]Current address: Laboratory for Visual Physiology, National Tokyo Medical Center, Higashigaoka 2-5-1, Meguro-ku, Tokyo 152-8902, Japan.
[2]Current address: Krieger Mind/Brain Institute, The Johns Hopkins Univ. 3400 N. Charles St., Baltimore, MD 21218, USA.

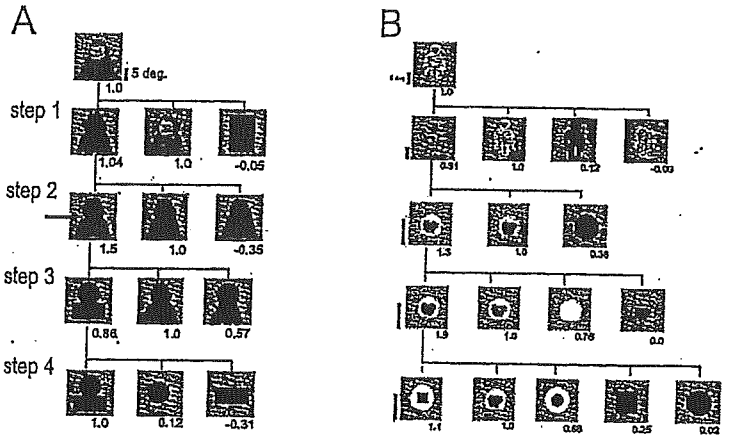

FIG. 1. The 'critical feature', a visual feature that maximally activates each cell, is determined by systematic stimulus simplification of the best object stimulus. First, we tested the cell with various 3D objects including faces, hands, stuffed animals, plastic fruits and vegetables, and paper mounts. After determining the best stimulus, we simplified it step by step to find the simplest stimulus that maximally activates the cell. For example in (A), at step 1, we compared the best coloured object with its silhouette, and found that the silhouette activated the cell equally well. The rightmost rectangle was taken as a control stimulus. The numbers below each picture indicate the response amplitudes normalized to the response to the reference stimulus, the best object. At step 2, we examined the effect of the 'sharpness' of the corner at the junction of upper and lower parts (arrow), and found that the silhouette with the sharp corners was the most effective stimulus. From left to right, the stimuli were the silhouette with sharp corners, the silhouette that evoked the best response at the previous step, the silhouette without corners. Further simplification was carried out at step 3. The leftmost stimulus evoked more than 70% of the response elicited by the best stimulus in the previous step, and was again examined in the next step as the reference stimulus. Finally at step 4, we determined the critical feature as a combination of a circle and a rectangle because neither the upper nor lower part alone activated the cell. Panel (B) shows another example of stimulus simplification where we found a dark square within a white circle as the critical features. (Y. Yamane and M. Tanifuji, unpublished observations.)

combinations of simple shapes, colours, luminance gradient/contrast, and textures. Although these features are more complex than the optimal visual stimuli for cells in areas V1, V2 and V4, they are still less complex than natural objects (Fig. 1).

Optical imaging to investigate distributed activity in area TE

Fujita and his colleagues showed that neurons with similar response properties are clustered into a column in area TE (Fujita et al 1992). Thus, intrinsic signal imaging of columnar activation can be used to investigate spatial patterns of activation (Tsunoda et al 2001, Wang et al 1996, 1998). This technique measures the decrease in the degree of light reflection elicited by neural activation from the exposed cortical surface using a CCD camera; the reflection changes are due to metabolic changes elicited by neural activation including changes in deoxygenation of haemoglobin in capillaries (Grinvald et al 1999). Intrinsic signal imaging in area TE

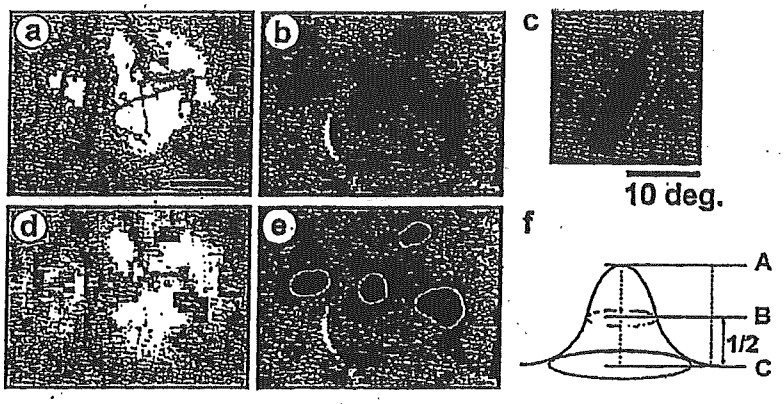

FIG. 2. Intrinsic signal imaging detects local modulation of light absorption changes in area TE. (a) Portion of area TE where intrinsic signals were recorded. (b) A differential image showing a local increase in absorption by the visual stimulus shown in (c). (d) Active spots, where the degree of reflection change evoked by the stimulus was significantly greater than that without the stimulus presentation. The region with the highest significance level is in black, and that with the lowest significant level in white ($P < 0.05$). (e) Active spots outlined by connecting pixels with 1/2 of the peak absorption value as in (f). (Modified from Tsunoda et al 2001.)

revealed that visual stimulus elicits local decrease of light reflection that appears as spots distributed across the cortex surface (Fig. 2) (Tsunoda et al 2001). Although these reflection changes are not a direct measure of neural activation, intrinsic signals coincide well with the activity of neurons examined by conventional extracellular recordings (Wang et al 1996, 1998, Tsunoda et al 2001). These spots, 'active spots', could correspond to a column of cells with similar responsiveness in this area (Fujita et al 1992).

Neural representations of object images in area TE

Intrinsic signal imaging with various object stimuli revealed that complex objects activate multiple spots (Fig. 3A). Some of the spots were commonly activated by different objects; other spots were specific for one of the examined stimulus. This observation is consistent with the idea that each of these spots could represent a particular visual feature as proposed previously. To examine this idea, we compared distribution patterns of spots activated by a complex object with those activated by systematically simplified stimuli (Fig. 3B) (Tsunoda et al 2001). We used a 'black cat' (a-*1*) as the complex object image and then simplified it to its 'head' (a-*2*), and to the 'silhouette of its head' (a-*3*). The original image (a-*1*) elicited fourteen spots, but presenting the 'head' (a-*2*) elicited only eight of the original 14 spots. The silhouette (a-*3*) only activated three (white) of the eight spots elicited by the head (a-*2*). Thus, the simplified stimulus lacking part of features in the original image activates only a subset of the spots elicited by the stimuli before simplification. Thus, individual spots represent visual features rather than object images in area

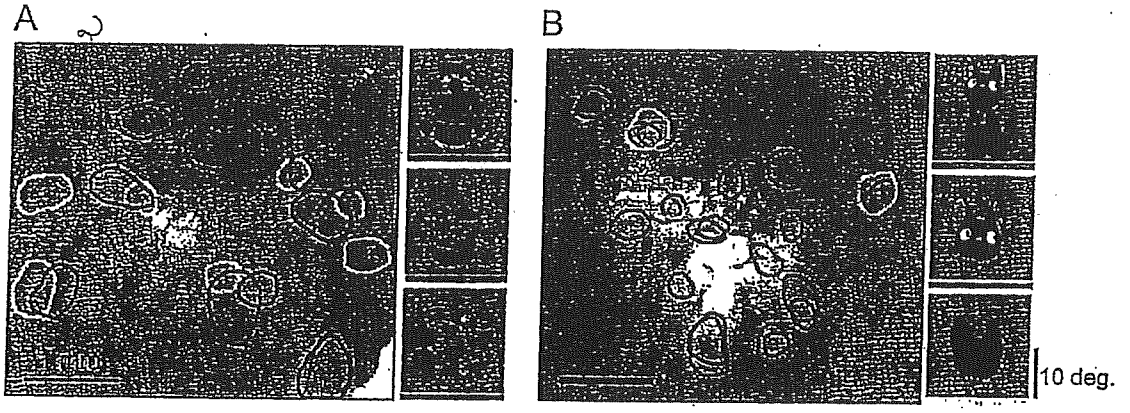

FIG. 3. Spatial patterns of activation elicited by complex object images are mapped on the image of the exposed cortical surface where the optical signals were recorded. (A) Activity in spots was elicited by three different object images. The colour of outlined spots and the line underneath the stimulus image are matched for the stimulus and the activated spots. (B) A case where simplified stimuli elicited only a subset of spots evoked by more complex stimuli.

TE. The actual visual features represented by individual spots were examined by extracellular recordings from neurons in active spots. For example, two spots (A, B) were activated by images of a fire extinguisher and a silhouette of it, but not by the fire extinguisher without handle and hose (Fig. 4). This difference in optical response patterns suggests that spots A and B represented visual features related to the handle and hose of the fire extinguisher. To confirm this expectation, we recorded extracellular responses from 25 cells in these spots shown in Figure 4, and analysed the response properties of the cells in each spot (Fig. 5). The handle and hose in isolation as well as the silhouette of the original fire extinguisher activated cells in spots A and B. The cells in spot A were also activated only by the handle having protrusions, but not by the hose alone. Furthermore, other stimuli with sharp protrusions, such as a 'hand' and 'cat's head' also activated the cells. Thus, the critical feature for the cells in spot A was 'sharp protrusions'. In contrast, cells in spot B were activated by the hose alone, but neither by the handle nor a 'line segment'. Thus, the critical feature for the cells in spot B was an 'asymmetric arc'. The cells in spot C were significantly activated by both the original fire extinguisher and the one without handle and hose. The simplest visual feature for cells in spot C was a 'rectangular shape', but cells also responded significantly to an 'ellipse'. Since there was no response to a 'circle', we determined the critical feature of the spots as an 'elongated structure'.

Representation of spatial arrangement of parts in object images

Examination of visual features represented by neurons in area TE suggested that at least some of the neurons in this area, represent 'local features' in object images,

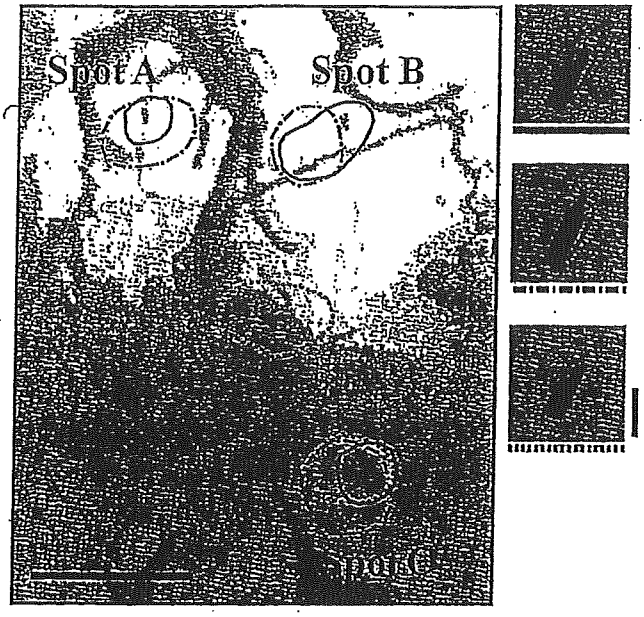

FIG. 4. A case shows that some spots (A and B) were activated by a fire extinguisher but not by the one without handle and hose. The spot at the center showed an opposite response pattern: activation with the fire extinguisher without handle but not by the original one. See Tsunoda et al (2001) for detailed analysis of the spot at the centre. Horizontal scale bars, 1 mm; vertical scale bar, 10 degrees.

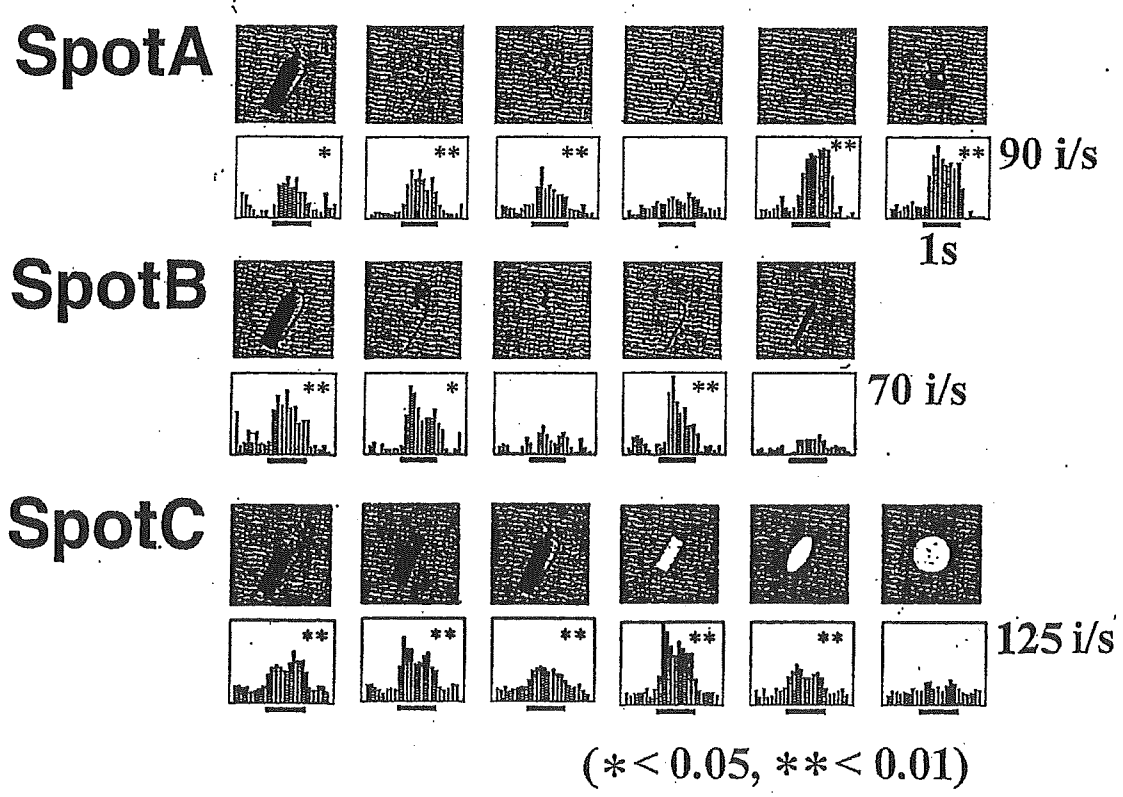

FIG. 5. Visual responsiveness of representative cells in spots A, B and C in Fig. 4. Adapted from Tsunoda et al (2001).

as neurons in spots A and B (Fig. 4) represent 'protrusions' and 'asymmetric curvature', respectively. Thus, information about the spatial arrangement of 'local features' is necessary for the specific representation of object images; some of the other spots may represent visual features related to the spatial arrangement of local features ('configurational information'). Here, we refer to 'local features' as visual features that occupy part of an object image and are distinguishable from other parts of an object image by their particular shapes, colours, or textures. 'Configurational information' is information about the spatial relationship of 'local features' themselves or about the spatial relationship of parts including local features. To examine the representation of 'configurational information', we investigated spots activated by an object (Original, Fig. 6-1) and the same object with a gap introduced between parts of the object (Fig. 6-4), but not by a part alone (Figs. 6-2 and 6-3) (Yamane et al 2001). These spots do not simply represent local features in objects because either part is not essential for activation. Moreover, activation by the stimulus with an introduced gap indicates that local features appearing at the junction of two parts, such as sharp connecting corners in Fig. 6-1, are also not essential. In three monkeys, we indeed found some of active spots had stimulus selectivity as described above. Extracellular recordings from cells in these spots showed that their critical features were combinations of vertically aligned two parts (Fig. 7a). In particular, the stimulus simplification procedure for these cells in this spot revealed that there was no activation by either part (for a representative case, see Fig. 1A). These cells were less sensitive to colour, texture, and local shapes of either part:

- there were no changes in the responses after removing colour and texture during the stimulus simplification procedure (Fig. 1A and 7a), and
- these cells responded equally well to object images even with different colour, texture, and local shapes, as long as the global configuration was similar to the critical features (Figs. 7b).

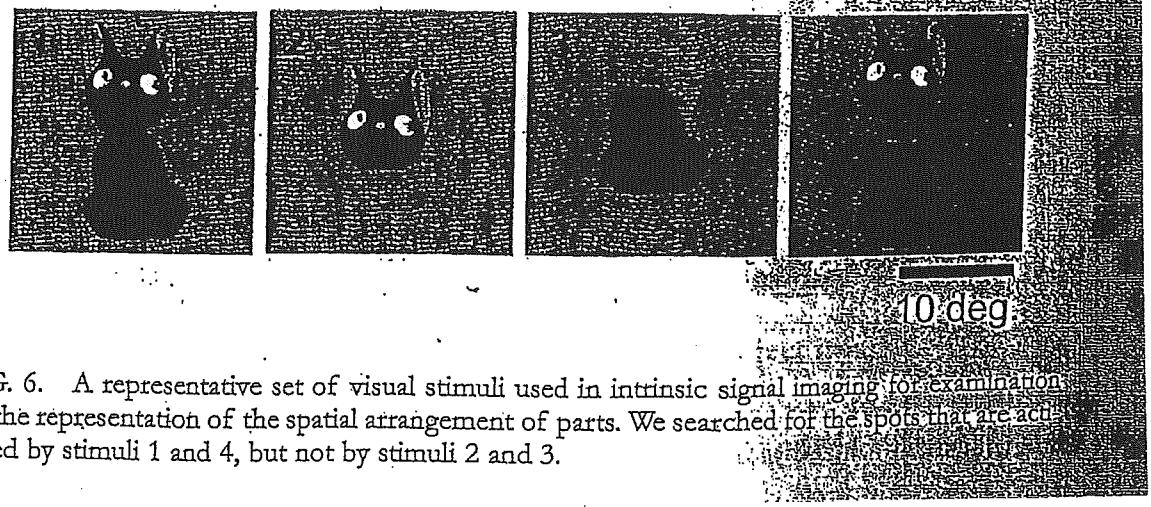

FIG. 6. A representative set of visual stimuli used in intrinsic signal imaging for examination of the representation of the spatial arrangement of parts. We searched for the spots that are activated by stimuli 1 and 4, but not by stimuli 2 and 3.

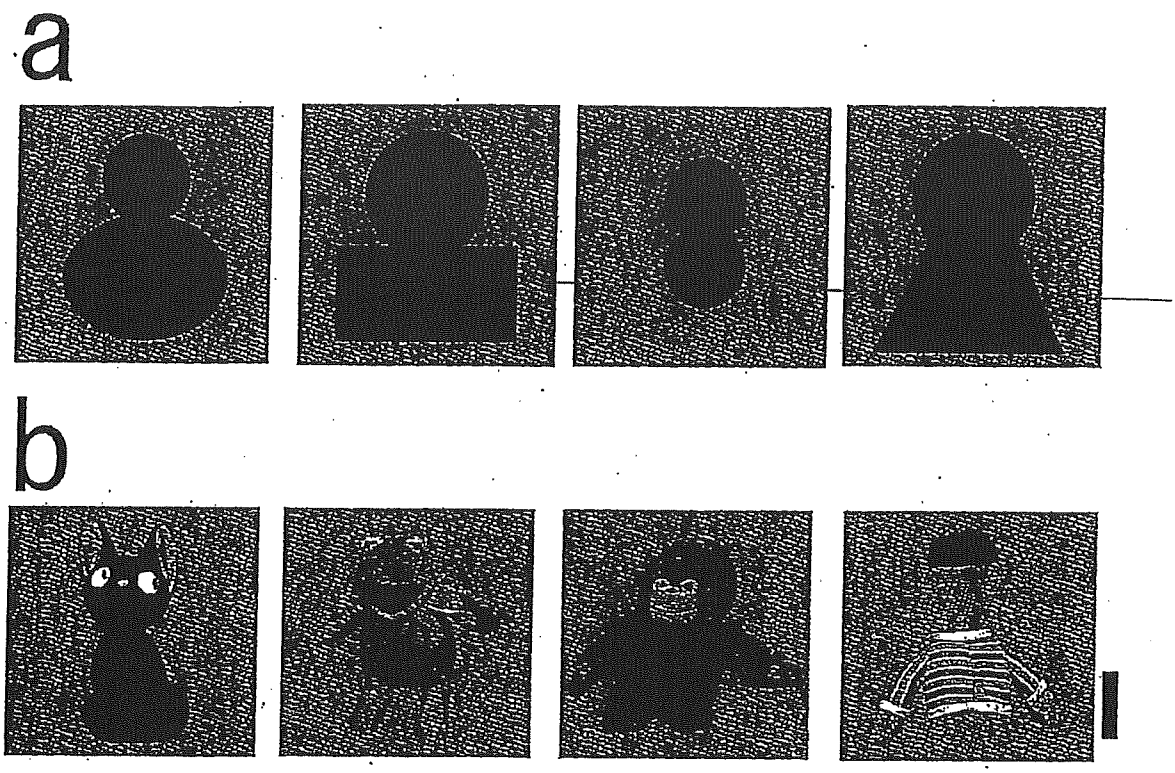

FIG. 7. Effective stimuli for neurons in a spot identified by the stimuli in Fig. 6. (a) Representative critical features determined by the stimulus simplification (Fig. 1). Please note that when colour and texture are not essential, the stimulus was filled black (see Fig. 1A). (b) The best object stimuli for these neurons, among 100 object stimuli examined before stimulus simplification. Scale bar, 5 degrees.

In contrast, we found that these cells were highly selective to a particular spatial arrangement of the upper and lower parts (Fig. 8).

Summary and conclusions

The combination of intrinsic signal imaging and extracellular recordings suggests that object images are represented as combinations of spots, and that each spot represents visual features less complex than the original object images (Figs. 4 and 5). These visual features are not specific for a certain object image but are common features across the wide range of object images. For example, spot A in Figure 4 represents 'sharp protrusions' that is a common feature among a fire extinguisher, hand and cat (Fig. 5 spot A). Thus, representation specific to object images requires combination of spots.

Spots do not necessarily represent 'local features' but some of them represent visual features related to object configurations. We found that neurons in these spots responded to visual stimuli consisting of vertically aligned upper and lower parts

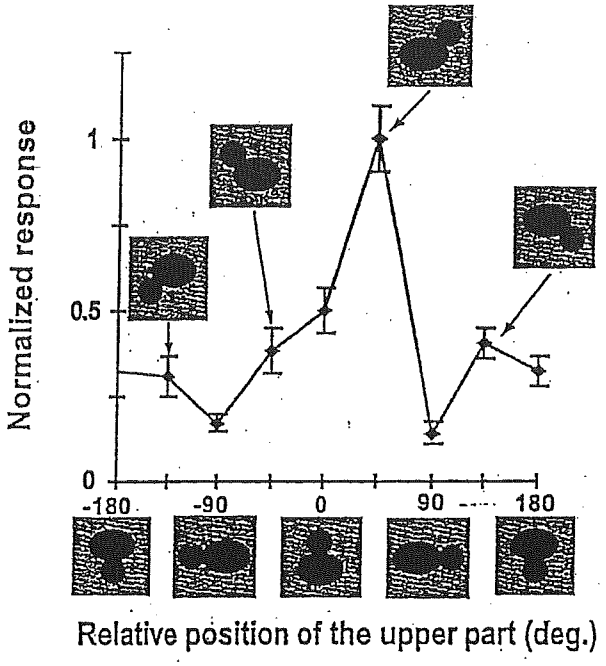

FIG. 8. Response specificity of a representative cell to the spatial arrangement of parts. The upper part of the critical feature of the cell was rotated relative to the lower part. The horizontal axis indicates the angle between the line connecting the center of upper and lower parts of each stimulus and that of the critical feature. The vertical axis indicates normalized value of stimulus evoked responses. In this particular case, the best response was elicited by the stimulus with 45 degrees, but many others respond maximally at 0 degrees.

(Fig. 8), but were less selective to local features embedded in either part (Figs. 1A and 7). We consider that such neurons specify the configuration of object images. Face neurons in area TE could play the same role. They respond specifically to a configuration specific for faces, but are less selective to individual faces (Desimone et al 1984, Perrett et al 1984, Baylis et al 1985, Yamane et al 1988, Young & Yamane 1992).

Although we made a distinction between local features and the spatial arrangement of parts in this text for clarity, we do not necessarily consider that neurons in area TE are generally categorized in two groups which represent either local features or spatial arrangement of parts. It is known that visual responses of neurons in inferior temporal cortex are modified by visual experience (Miyashita 1988, Logothetis et al 1995, Kobatake et al 1998), and we consider that visual features represented by neurons are shaped based on the statistical nature of the visual environment. A single neuron could represent partly global and partly local features if such a combination appears frequently in the visual environment. We observed neurons representing local features such as protrusion and curvature, those representing vertically aligned two parts, and those responding to faces, because these features are common in the natural visual environment.

Finally, in relation to action, our present knowledge about representation of object images in area TE may not be sufficient. Although our investigations suggest that multiple spots representing visual features of an object image are necessary to specifically represent the object image, we may not need complete representations of object images in a behavioural context. Investigations described here with behaving animals are required in future.

Acknowledgments

This work was partly supported by Research Fellowships of the Japan Society for the Promotion of Young Scientists to Y. Y.

References

Baylis GC, Rolls ET, Leonard CM 1985 Selectivity between faces in the responses of a population of neurons in the cortex in the superior temporal sulcus of the monkey. Brain Res 342:91–102

Desimone R, Albright TD, Gross CG, Bruce C 1984 Stimulus-selective properties of inferior temporal neurons in the macaque. J Neurosci 4:2051–2062

Fujita I, Tanaka K, Ito M, Cheng K 1992 Columns for visual features of objects in monkey inferotemporal cortex. Nature 360:343–346

Grinvald A, Shoham D, Shmuel A et al 1999 In-vivo optical imaging of cortical architecture and dynamics. In: Windhorst U, Johansson H (eds) Modern techniques in neuroscience research. Springer, Berlin, p 893–970

Kobatake E, Tanaka K 1994 Neuronal selectivities to complex object features in the ventral visual pathway of the macaque cerebral cortex. J Neurophysiol 71:856–867

Kobatake E, Wang G, Tanaka K 1998 Effect of shape-discrimination training on the selectivity of inferotemporal cells in adult monkeys. J Neurophysiol 80:324–330

Miyashita Y 1988 Neuronal correlate of visual associative long-term memory in the primate temporal cortex. Nature 335:817–820

Logothetis NK, Pauls J, Poggio T 1995 Shape representation in the inferior temporal cortex of monkeys. Curr Biol 5:552–563

Perrett DI, Smith PAJ, Potter DD et al 1984 Neurons responsive to faces in the temporal cortex: studies of functional organization, sensitivity to identity and relation to perception. Hum Neurobiol 3:197–208

Tanaka K, Saito H, Fukada Y, Moriya M 1991 Coding visual images of objects in the inferotemporal cortex of the macaque monkey. J Neurophysiol 66:170–189

Tsunoda K, Yamane Y, Nishizaki M, Tanifuji M 2001 Complex objects are represented in macaque inferotemporal cortex by the combination of feature columns. Nat Neurosci 4:832–838

Wang G, Tanaka K, Tanifuji M 1996 Optical imaging of functional organization in the monkey inferotemporal cortex. Science 272:1665–1668

Wang G, Tanifuji M, Tanaka K 1998 Functional architecture in monkey inferotemporal cortex revealed by in vivo optical imaging. Neurosci Res 32:33–46

Yamane S, Kaji S, Kawano K 1988 What facial features activate face neurons in the inferotemporal cortex of the monkey? Exp Brain Res 73:209–214

Yamane Y, Tsunoda K, Matsumoto M, Phillips A, Tanifuji M 2001 Decomposition of object images by feature columns in macaque inferotemporal cortex. Soc Neurosci Abstr 27:1050

Young MP, Yamane S 1992 Sparse population coding of faces in the inferotemporal cortex. Science 256:1327–1331

DISCUSSION

Esteky: When you choose a spot in your optical imaging and stick the electrode in, do you select a neuron that is responsive to the stimulus you are using, or do you randomly select any neuron? In a given cortical column in inferior temporal cortex (IT) there are a variety of cells responsive to many different kinds of stimuli. So you are not dealing with a uniform and homogeneous cortical spot. Do you select the stimuli that fit your optical imaging results?

Tanifuji: No. We were only biased to neurons which gave visual responses. In other words, we didn't examine neurons that didn't reveal any visual responses. Here, visual responses were examined for about 100 3D objects. These objects were manually presented to animals. This procedure allowed us to show more than 100 visual stimuli, because each object was presented at different viewing angles.

Esteky: Was there always a good correspondence between the optical imaging data and the single unit data, or were there inconsistencies?

Tanifuji: It depends on spots. The correlation is very high in some spots where more than 90% of neurons show response consistent with the result of optical imaging. However, in other cases, the percentage is as low as 60%. But if we randomly select neurons regardless of the location of spots, the number of neurons responding to the stimuli that activated a certain spot is less than 30%. The value, 60% means that there is some clustering of neurons with similar response property, and thus we could see activated spots by optical imaging. I somehow wonder whether there could be strong and weak columns depending on how variable the response properties of neurons within the columns are.

Logothetis: I have a general question regarding work with different types of shape descriptions. I know how tedious it is to do this kind of work. Were you able to get a sense of what kind of variability and among what kinds of dimensions this variability is in single spots? If you have two or three presentations in approximately the same position could you say what kind of variability you found with this systematic approach?

Tanifuji: It is very difficult to explain in a few words.

Albright: I assume you are talking about variability across neurons. These things are 500 microns across. It can't possibly be the case that there are consistent properties within that entire region. In our experience you can go from one neuron to the next and find a completely different set of recordings.

Logothetis: So if you get the parameters of the first two coefficients of the Fourier descriptors you are using, you find huge discontinuity.

Albright: Yes, which is somewhat inconsistent with this notion of columns in IT. The columns are categorical, but within one of those columns there is a great deal of variability. We don't know what the relevant variables are.

Logothetis: In defining these columns, there is a process of categorization on the part of the experimenter. I see a certain computationally dangerous arbitrariness. There is not much of a systematic basis to what you see. One has a tendency to say there is a column there. What would be the definition of the column if we wanted to call these spots a column?

Tanifuji: Let me explain a simple experiment we did. We examined the correlation of selectivity for 100 objects for nearby neurons. Then, we found the correlation coefficient for the stimulus selectivity is 0.4. Though it is not very high, this value is still statistically significant.

Albright: Are the two neurons adjacent to one another in successive recordings?

Tanifuji: Yes. The pairs were placed near each other. The distance was approximately 150 μm.

Logothetis: Have you tried to do the best possible isolation of these neurons. Sometimes an 'isolated' neuron is 2mV.

Tanifuji: We isolate the cell with the standard template matching. I think there is no particular bias to large or small cells. We analysed multiple cellular activities as well.

Logothetis: Have you tried to do the unit responses?

Tanifuji: Yes. I should point out one thing. Although a correlation coefficient of 0.4 is statistically significant, looking at the best object stimulus of individual cells, they are different. As reported by Ichiro Fujita and Keiji Tanaka (1992), however, the critical features of individual cells are very similar. We consider that although the object selectivity of nearby neurons is different, this is because the tuning broadness around the optimal stimulus is not the same for different neurons, and that the optimal stimuli, namely critical features, themselves are the same for nearby cells.

Logothetis: You said that there is a 0.4 correlation between the arbitrary tuning curves. This means that you only explain 16% of the variance. Would you call this a column? Tom Albright, do you remember what the situation was with MT?

Albright: It is better than 0.4. I want to make sure what the measurement is here. You have 100 stimuli and the correlation for responses across neurons is 0.4 for neurons within the same module. What is it if you have one within a module and another outside?

Tanifuji: Then, the correlation coefficient dropped down to around 0.1.

Esteky: On average, some 15% of stimulus images evoke significant responses in an IT cell. This suggests a rather wide shape tuning in IT. The wide tuning is true even for cells known to respond 'selectively' to faces: single unit recordings and fMRI studies have shown that face cortical cells/modules also respond to non-face stimuli.

Tanifuji: If neurons that respond to a particular stimulus are homogeneously distributed across the cortex, then optical imaging with the stimulus would not show

any spots. Appearance of spots means that there is clustering of neurons at least for those that respond to that particular stimulus. One thing that is uncertain is how much darkening we could obtain if all the neurons within a spot are activated. Thus, even if darkening of a spot is observed with a stimulus, optical imaging experiments could not say anything about a possibility that some neurons in the spots did not respond to the stimulus but to others.

Esteky: Your approach does not reveal whether you are dealing with specific spots that respond exclusively to the selected stimulus or spots that are more widely tuned. In other words, in addition to showing that a stimulus is effective in activating a particular column or a cell (i.e. response selectivity) one needs to show how specific or exclusive the cells respond to that particular stimulus (i.e. response specificity). The correlation difference that you get in distant columns depends on the type of visual images used in your stimulus set. If the images contain a wide range of common or simple features a lower difference would be expected and vice versa.

Tanifuji: Of course different objects could activate the same cell. The question is whether this is because the cell is broadly tuned to these objects or the cell is tuned to a feature that is common to these objects, even though these objects look very different. In the case of the fire extinguisher, I showed a cell (spot A) that responded to the fire extinguisher, a hand, and the cat's head. These objects are different, but responses to these objects were easily explained by the cell's specific responses to 'protrusions'. We can not exclude the former possibility, but at least this result favours the latter possibility.

Let me say something more about the object selectivity. We compared object selectivity for nearby neurons and found that the correlation coefficient of stimulus selectivity for nearby cells is something like 0.4. This means that there is a statistically significant correlation in stimulus selectivity of cells, but it also means that the tuning curves of nearby cells are different to some extent. Then, one might imagine that the averaged activity of all the neurons in a column will lose stimulus specificity, or the tuning curve of averaged activity would not be as sharp as that of individual neurons. However, we found that this is not the case. We recorded many neurons in the same spot, and averaged neurons' activities for individual object to generate super multiple cellular activity. Next, we compared sharpness of object selectivity for super-multiple cellular activity, for single cellular responses, and for multiple cellular activities (MUA at a site). Interestingly, the sharpness of the object selectivity is almost the same for these three cases. Based on this observation, we think there is a certain feature that represents the spot, but this feature could not be simply captured by the result of object selectivity from one or two constituent neurons in the spot. The reason is that, in addition to common response property of the spot, individual cells have their own tuning variability, and that the variability in individual cells masks the common property of the spot in the object selectivity experiment. One way to capture the columnar level property is to use the